# A finite element model of the mechanical interactions between peripheral nerves and intrafascicular implants

Journal of Neural Engineering

PAPER

# A finite element model of the mechanical interactions between peripheral nerves and intrafascicular implants

**Outman Akouissi**[1,2,*], **Stéphanie P Lacour**[1,5], **Silvestro Micera**[2,3,5] **and Antonio DeSimone**[3,4,5,*]

[1] Bertarelli Foundation Chair in Neuroprosthetic Technology, Laboratory for Soft Bioelectronic Interfaces, Neuro-X Institute, Ecole Polytechnique Fédérale de Lausanne (EPFL), Geneva, 1202, Switzerland
[2] Bertarelli Foundation Chair in Translational Neuroengineering, Translational Neural Engineering Laboratory, Neuro-X Institute, Ecole Polytechnique Fédérale de Lausanne (EPFL), Geneva, 1202, Switzerland
[3] The Biorobotics Institute and Department of Excellence in Robotics & AI, Health Science Interdisciplinary Center, Scuola Superiore Sant'Anna, Pisa, Italy
[4] SISSA—International School for Advanced Studies, 34136 Trieste, Italy
[5] Authors contributed equally to the work.
[*] Authors to whom any correspondence should be addressed.

**E-mail:** outman.akouissi@epfl.ch **and** desimone@sissa.it

**Keywords:** peripheral nerves, finite element modeling, implant mechanics, foreign body reaction, peripheral nerve interfaces

Supplementary material for this article is available online

OPEN ACCESS

RECEIVED
28 July 2021

REVISED
19 June 2022

ACCEPTED FOR PUBLICATION
29 June 2022

PUBLISHED
21 July 2022



## Abstract

*Objective.* Intrafascicular peripheral nerve implants are key components in the development of bidirectional neuroprostheses such as touch-enabled bionic limbs for amputees. However, the durability of such interfaces is hindered by the immune response following the implantation. Among the causes linked to such reaction, the mechanical mismatch between host nerve and implant is thought to play a decisive role, especially in chronic settings. *Approach.* Here we focus on modeling mechanical stresses induced on the peripheral nerve by the implant's micromotion using finite element analysis. Through multiple parametric sweeps, we analyze the role of the implant's material, geometry (aspect-ratio and shape), and surface coating, deriving a set of parameters for the design of better-integrated implants. *Main results.* Our results indicate that peripheral nerve implants should be designed and manufactured with smooth edges, using materials at most three orders of magnitude stiffer than the nerve, and with innovative geometries to redistribute micromotion-associated loads to less delicate parts of the nerve such as the epineurium. *Significance.* Overall, our model is a useful tool for the peripheral nerve implant designer that is mindful of the importance of implant mechanics for long term applications.

## 1. Introduction

Peripheral nerve interfaces (PNIs) have allowed remarkable achievements, from closed-loop control of prosthetic limbs to novel electroceutical therapies [1–5]. PNIs are grouped into three main design categories of increasing order of invasiveness and selectivity: (a) extraneural, surrounding the nerve, (b) intraneural (or intrafascicular), penetrating the nerve, and (c) regenerative, exploiting the repairing mechanisms of transected nerves [6]. Most implants interact with the nerve through the stimulation and recording of electrical signals [7–10], but chemical and optical modalities have been recently demonstrated [11–13]. The chronic performance, from a few months to several years, of all these devices is hindered by the foreign body reaction (FBR) triggered by the subject's immune system, causing the formation of scar tissue and the secretion of aggressive chemicals that hamper the implants' electrical and mechanical properties, often leading to their failure [14–17]. The intensity of the FBR, that includes the thickness of the scar and the degree of inflammation around the implant [18], is exacerbated by the invasiveness of the PNI and is of critical importance for the long-term functioning of neuroprostheses relying on intrafascicular implants [19]. While the causes leading to the onset and worsening of the FBR over time are being investigated by the neuroprosthetics community, multiple hypotheses have been formulated, some of which have been confirmed experimentally. For example, it is well known that the FBR is initiated immediately following implantation: the trauma caused by the placement of the implant, characterized

by tissue laceration and blood vessel shearing, triggers the secretion of chemokines recruiting immune cells that surround and attack the implant [20, 21]. At the same time, the FBR evolution and worsening over time is attributed to multiple factors, among which there is the mechanical mismatch between (soft) nerves and (stiffer) implants: while the first are characterized by highly non-linear anisotropic mechanical properties, with elastic moduli lower than 1 kPa under small strains, the materials used to fabricate PNIs are orders of magnitude stiffer (∼5 GPa for polyimide [8, 22, 23] and ∼1 MPa for silicone elastomers [24–26]). Moreover, these devices operate in a harsh environment where they are subject to repeated mechanical stimuli such as the pulling forces exerted by connecting cables and contraction forces applied by the nearby contracting muscles [14, 27]. The mechanical mismatch combined with the repeated external forces induce stresses on the nervous tissue, bolstering the inflammation at the implantation site [28]. Researchers have therefore developed different approaches to reduce the nerve-implant mechanical mismatch, replacing stiff polymers with softer elastomers [29, 30], or including coatings with soft materials such as hydrogels or antifouling polymers [31–34]. However, most of these examples are dedicated to the least invasive and least selective extraneural implants and little research is available on the minimum requirements to reduce such phenomenon when using intraneural implants [30]. The mechanical mismatch theory is therefore considered a reasonable hypothesis that deserves further experimental studies, especially when focusing on more invasive intrafascicular implants.

Until now, mechanical optimization of PNIs has been performed in a trial and error fashion through lengthy and complicated surgeries in numerous animals. As an alternative solution, finite element models (FEMs) have been used as a tool to guide the design of neural interfaces, in particular simulating the electrical interaction between nerves and intrafascicular electrodes but also the mechanical interaction between brain and cortical implants. In the first case, FEMs have been developed to simulate the distribution of applied electric fields that have been then used to derive the selectivity in stimulation [35–39]. In the second case, FEMs have been used to study the induced stresses and strains on the brain by intracortical implants of different elastic moduli [40, 41]. Altogether finite element modeling is a valuable tool for the design of implants prior to *in vivo* evaluation, leading to durable devices and reducing the number of required animals for testing. However, the full potential of FEMs for the mechanical optimization of PNIs remains untapped. This kind of study could provide important indications about the most promising materials and designs that can be used to minimize the effects of mechanical mismatch between nerves and PNIs. Inspired by these examples, we have developed simplified FEMs simulating the mechanical interaction between a rodent's sciatic nerve and an intraneural implant. Focusing on the implant's micromotion originating from connecting wires and limb movement, we have explored possible approaches to reduce induced stresses and strains on the host nerve. Although the nerve-implant interface is extremely complex in terms of nerve anatomy, mechanical properties, and external stimuli, we expect to derive essential indications on the most promising implant designs and materials with our simplified models. We have investigated the effects of the elastic modulus of the implant material (from 1 GPa to 1 kPa), the form of the material (bulk or coating) together with implant aspect ratio and hybrid geometries. The results we have obtained provide a series of guidelines on the most promising approaches that can reduce stress transmission on the nerve, guiding the implant designer in the choice of both materials and geometry of future PNIs.

## 2. Methods

We decided to simulate the behavior of intraneural electrodes in the rat's sciatic nerve, the most used model when testing peripheral nerve implants. The FEM study is performed using a desktop PC (Windows 10, Intel Xeon E5-1607 CPU @ 3 GHz, 64 GB RAM). COMSOL 5.6 (Build 280) is used, with the Solid mechanics and the MEMS modules. The geometry is built using the standard tools available in the software. The mesh is built manually, starting from a triangular 2D mesh of the nerve-implant interface, refined along the shortest edges (>2 $\mu$m per triangle side). A free tetrahedral mesh is used, with a volume distribution increasing distally from the interface (maximum growth rate > 1.6). The number of tetrahedral elements is approximately $5 \times 10^5$, with average volume of 1 ml. A linear direct solver is used, together with a constant Newton non-linear method with a damping factor of 1. Termination is tolerance based, using the residual as termination criterion. Run time is approximately 10 min per parameter. We have designed a 3D model comprising three fascicles embedded in an interfascicular epineurium that is itself wrapped around by an external epineurium. The morphology and dimensions used in our model take inspiration from the rich literature including histological images [35, 42, 43]. Using a simplified geometry, all components of the nerve have an elliptical shape with a long and short axis, as shown in figure 1. The fascicles have three different axes-pairs ($\mu$m × $\mu$m): 1000 × 600, 400 × 600 and 1500 × 900. The interfascicular epineurium, in which the fascicles are embedded, is 2120 $\mu$m wide and 1900 $\mu$m high. Finally, the external epineurium covers the outer surface of the interfascicular one, with a thickness of 80 $\mu$m. We did not include the perineurium layer around each fascicle as its reduced

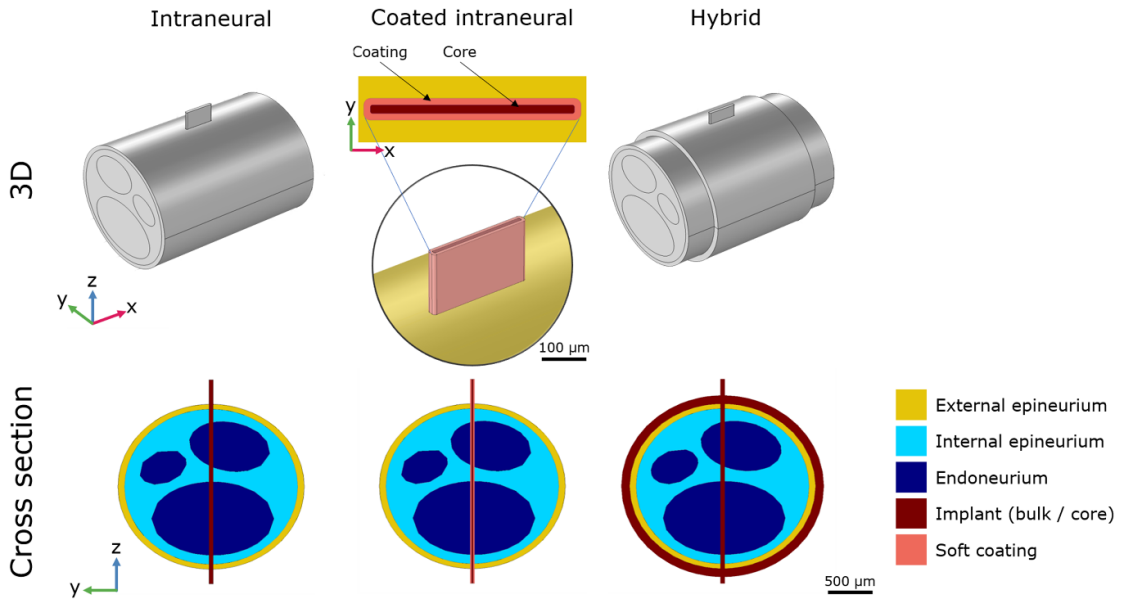


**Figure 1.** 3D geometries of the models studied with the relative cross sections displaying the materials used and the interface geometry at the YZ midplane.

thickness (in the range of 5–10 $\mu$m) would considerably increase the complexity of the model without any significant difference in the mechanical response of the nerve. The resulting 2D geometry is then extruded normally for a thickness of 3 mm, this reduced length is considered when formulating the boundary conditions of the simulations. Overall, the modeled nerve is 3 mm long ($X$-axis), 2280 $\mu$m wide ($Y$-axis), and 2060 $\mu$m tall ($Z$-axis). We have simulated a penetrating implant similar to the transversal intrafascicular multichannel electrode (TIME) [7], using a rectangular bar crossing external and interfascicular epineurium and two fascicles. The implant is 500 $\mu$m wide ($X$-axis), 50 $\mu$m thick ($Y$-axis) and 2.5 mm long ($Z$-axis), therefore piercing through the entire nerve, and is oriented along the extrusion axis of the nerve. To reduce the effect of singularities caused by sharp corners in the implant's geometry, the four long edges are filleted with a radius of 15 $\mu$m. The top surface of the implant, where all displacements are applied, is 300 $\mu$m above the surface of the nerve. The thickness of the implant is chosen to be twice that of a standard polyimide-based TIME as a [7], this will accommodate also softer materials as they are usually thicker for handling purposes. We have neglected the presence of thin metal film tracks and other details for the sake of simplicity and pertinence to the study [44]. Note that the terms used to describe dimensions refer to different orientations when associated to the nerve or the implants.

To verify the effect of thin and thick coatings on flexible implants yet stiffer, we have included a homogeneous coating layer with thicknesses of 5, 10, 15, 20 and 22.5 $\mu$m. Overall, the footprint of the implant is constant and identical to the regular TIME implant, meaning that the core changes of dimensions depending on the thickness of the coating. We have performed FEM studies of TIME implants while varying their cross-sectional aspect ratio: thanks to our simulations we could verify the stresses applied on the nerve by thinner or narrower penetrating electrodes. We therefore simulated the behavior of implants with thicknesses of 100, 200, 300, 400 and 500 $\mu$m and widths of 10, 20, 30, 40 and 50 $\mu$m, while applying an identical set of boundary conditions as in the first group of TIME studies. We have also implemented a new implant geometry that includes an intrafascicular part, identical to the TIME, and an extraneural cuff-like part that wraps around the nerve at the implantation site to understand the potentials of this 'hybrid' approach. The two parts are welded together via a union operation. The extraneural cuff part of the implant has a thickness of 100 $\mu$m, a length of 2 mm and is centered around the intrafascicular part. The implant parameters used in this study are summarized in table 1.

### 2.1. Boundary conditions and study settings

The goal of the simulations is to infer contributions of implant stiffness on the stresses and strains induced to the nerve. For this reason, we have selected boundary conditions to reproduce the mechanical environment and stimuli experienced by the rat's peripheral nerve. Following our experience in isolating the sciatic nerve in rats, exposing it until the distal trifurcation, we set the length of the nerve to be of 15 mm, without any change in size or ramification along its length. To further speed up solving time, we implement a model with a shorter nerve, 3 mm long, and added a *spring foundation* boundary condition with elastic coefficients given by the materials' properties and the length of the connection: this is equivalent

**Table 1.** List of the implant parameters varied in the finite element models in this study.

| Parameter | Values | Other settings |
|---|---|---|
| Bulk implant modulus | 1 kPa, 10 kPa, 100 kPa, 1 GPa | Fixed cross section: 500 × 50 $\mu$m |
| Soft coating thickness | 5, 10, 15, 20, 22.5 $\mu$m | Fixed cross section: 500 × 50 $\mu$m<br>Coating modulus: 1 kPa<br>Core modulus: 1 GPa |
| Implant thickness | 10, 30, 50 $\mu$m | Modulus: 1 GPa<br>Width: 500 $\mu$m |
| Implant width | 100, 300, 500 $\mu$m | Modulus: 1 GPa<br>Thickness: 50 $\mu$m |
| Hybrid implant modulus | 1 kPa, 10 kPa, 100 kPa, 1 GPa | Fixed cross section: 500 × 50 $\mu$m<br>Cuff thickness: 100 $\mu$m |

to having a fixed constraint at the extremities of a 15 mm nerve. We therefore saw no difference between the full 15 mm geometry and the shortened geometry in a randomly selected subset of studies. The interface between implant and nerve can be characterized by different adhesive or frictional properties. In reality, the characteristics of this interface depend on a large number of variables such as material roughness, stiffness, wetting, and more. To simplify the study, we choose to simulate an interface characterized by fully adherent surfaces. This constitutes the worst-case scenario when considering the stresses and strains induced on the nerve, as all external stimuli are transmitted to the nerve without any losses or slipping. Since the implant pierces through the entire nerve, this assumption is compatible with our study setup. This approach is also used when simulating the behavior of the hybrid electrode and its extraneural component, that is considered fully adherent to the epineurium. In COMSOL, we implement such condition by applying an identity mapping pair linking the outer surface of the implant to the adjacent neural tissue. Peripheral nerve implants can be subject to external forces due to the cables linking the device to external interfaces. Implants therefore can exert stresses on the nerve during limb movement, causing damage at the interface and potentially worsening the FBR. In our models, we simulate the consequences of tethering forces by applying prescribed displacements at the upper extremity of the implant. We individually evaluate a representative displacement of 20 $\mu$m along each axis, constraining any other movement in the two remaining directions. Peripheral nerves, like other biological tissues, show highly complex mechanical properties such as viscoelasticity, hyperelasticity and poroelasticity that originate from the intricate interaction between different cells, extracellular matrix and blood vessels [45–49]. In our model, we evaluate a simplified version of the problem by considering the behavior of the nerve as elastic in the small strain regime (<5%). We neglect viscous and nonlinear effects, focusing on the linearly elastic ones by setting up a standard stationary study that evaluates stresses and strains at equilibrium.

### 2.2. Materials

Each component of the simulation is characterized by mechanical properties linked to an assigned material. Given the scope of our study, we have chosen to model all components used in our analysis as linear elastic materials. This simplification is possible thanks to the assumption of operation within the small (<5%) strain domain, neglecting all viscous and nonlinear mechanical contributions. To further simplify the model, in the simulated volume of the nerve, we assigned a tissue-specific Young's modulus to each component. All materials therefore are characterized by an elastic (Young's) modulus and a Poisson ratio. Since biological tissues are characterized by their high water content, all nerve components are considered to made of be incompressible materials and therefore have a Poisson ratio of 0.49. In this study, we evaluated the stresses arising following a 20 $\mu$m displacement at the top of an intrafascicular implant. Given the small magnitude of the external disturbance, the anisotropic nature of the fascicles can be neglected as also the bands of Fontana are features in the same scale [50]. On the other side, the elongated geometry of the nerve in our model induces the largest differences in the response to displacements in the *X, Y* and *Z* directions. We therefore decided to simplify the model by modeling the tissues as isotropic, as done in other FEM studies [45, 51]. The materials used to simulate the implants are characterized by Young's moduli ranging from 1 GPa to 1 kPa. Each value represents the mechanical properties of materials commonly used in PNIs, starting from flexible polymers such as polyimide [7, 10], going through stretchable silicone elastomers [26, 30, 52] to finally simulate soft biomimetic hydrogels [29, 32]. The implants are characterized by a Poisson ratio of 0.3 for the 1 GPa material (inspired by polyimides) or a Poisson ratio of 0.49 for the remaining cases. When evaluating the effects of implant coatings with different thicknesses, the core of the device is constituted of a material with Young's modulus of 1 GPa and Poisson ratio of 0.3, while the coatings have a fixed modulus of 1 kPa and Poisson ratio of 0.49. Mechanical properties of nerves have been a subject of study in different

fields such as physiotherapy, surgery and, recently, neuroprosthetics. The measured properties unfortunately highly depend on the methods (tensile, compressive, shear elastography, …) and scales (whole nerve, single axon, …) at which they are obtained [53]. Additional variance comes from the mechanical differences correlated with the animal model used, its age and the conditions of the measurement (*in vivo*, *ex vivo*) [54]. In our model, we have chosen to consider elastic moduli obtained by indentation with an atomic force microscope (AFM) tip from previous studies [31, 55]: given the scope of the study, that is to evaluate strains and stresses at the very interface between nerve and implant, measurements at the micron-scale are the most pertinent to our goal. The spatial resolution of the AFM enables the mapping of the distinct components of the nerve e.g. axons, epineurium etc, which can in turn be simulated in the model. The methods used correspond to those already used by Rosso and Guck [54]. We assigned a Young's modulus of 90 Pa to the fascicles, 60 Pa to the interfascicular epineurium and 140 Pa to the external epineurium.

### 2.3. Stress evaluation

To understand the effect of implant stiffness on the stresses and strains induced on the nerve, we have evaluated the von Mises stress. Figures 2–5 display the behavior of the Von Mises stress, simply called 'stress' from now on. In order to deduce the most stringent criteria for minimizing the stresses induced on the nerve, we evaluated the maximum stress values and the positions at which they occur, together with the average stress across the entire nerve-implant interface. However, the sharp changes in geometry and elastic properties in our model cause the occurrence of numerical artifacts, such as singularities at the top entry point of the implant into the nerve. Peak stresses and strains in the fascicles, far from the entry point, are instead unaltered by these uncertainties and are physically meaningful. We therefore evaluate the maximum stress on the internal fascicle-nerve interface and the average stress at the whole nerve-implant interface. The latter is calculated by first evaluating the total stress on a surface offset by 100 $\mu$m from the interface, where the effect of singularities has faded away, and then by dividing it by the area of the original interface. The total stress transferred from the implant to the nerve is independent from the distance at which it is evaluated, therefore the offset of 100 $\mu$m is chosen as the smallest one guaranteeing that stress and strain on the offset surface are unaltered by further mesh refinement. All quantities are evaluated using the built-in functions available in COMSOL. Given the simplifications and assumptions adopted in this work, the absolute values of the resulting stresses could not carry realistic and meaningful information per se. Instead, for each parametric study, we have focused on the relative variation of the resulting average stress on the nerve-implant interface and maximum stress on the fascicles, as it is found in brain-related biomechanical FEM studies [40, 41]. Therefore, each set of results is normalized with respect to the value (average on the whole interface or max stress at fascicle-implant interface) measured in the case of a standard implant, with a Young's modulus of 1 GPa and a cross-section of 500 $\mu$m by 50 $\mu$m, displaced along the $X$-axis. To facilitate visualization, the deformation in all the cross-section plots is amplified by a factor of 15.

## 3. Results

### 3.1. Bulk intrafascicular implant

The first set of models aims at simulating the behavior of a single-shank intrafascicular probe, inspired by the TIME device. The consequences following the displacement at the top of the implant are therefore analyzed as described in the previous section. Studying the effect of 20 $\mu$m displacements prescribed at the top of the implant, we evaluated the maximum Von Mises stress at the fascicles and the average ever the entire interface. The cross-sections in figure 2 show the stress distribution and deformation in the nerve following the displacement at the top of the implant. It can be noticed that softer implants tend to deform close to the implantation entry point, owing to their greater compliance, concentrating stress in the same area. Plotting the Von Mises stress as a function of implant modulus and displacement direction, important trends and differences between each case can be noticed. In fact, the highest stresses are caused by displacements along the nerve's axis ($X$ axis), as the smallest side of the implant (50 $\mu$m wide) applies forces that are concentrated on a smaller area. The plot also shows that the average stress at the interface decreases only when the stiffness of the implant is below 100 kPa, a value three orders of magnitude higher than the nerve's components. The trend is similar for all displacement cases, along the $X$ axis. Implants with a modulus of 1 kPa can therefore cause maximal stresses more than 50% lower than the ones caused by their rigid counterparts. The stress distribution along a cutline passing through the nerve, parallel to and 5 $\mu$m away from the rounded edge of the implant, shows how stresses are distributed along the length of the interface passing through the point where the maximum values are located. The plots show that the stresses induced by soft implants concentrate at the entry point, on the epineurium mostly, to rapidly decay along the length, applying stresses on fascicles that are lower than the ones caused by stiff implants. This behavior is most prominent when considering displacements along the $Y$ axis, as the bending of the softer device causes important stress concentrations at the top.

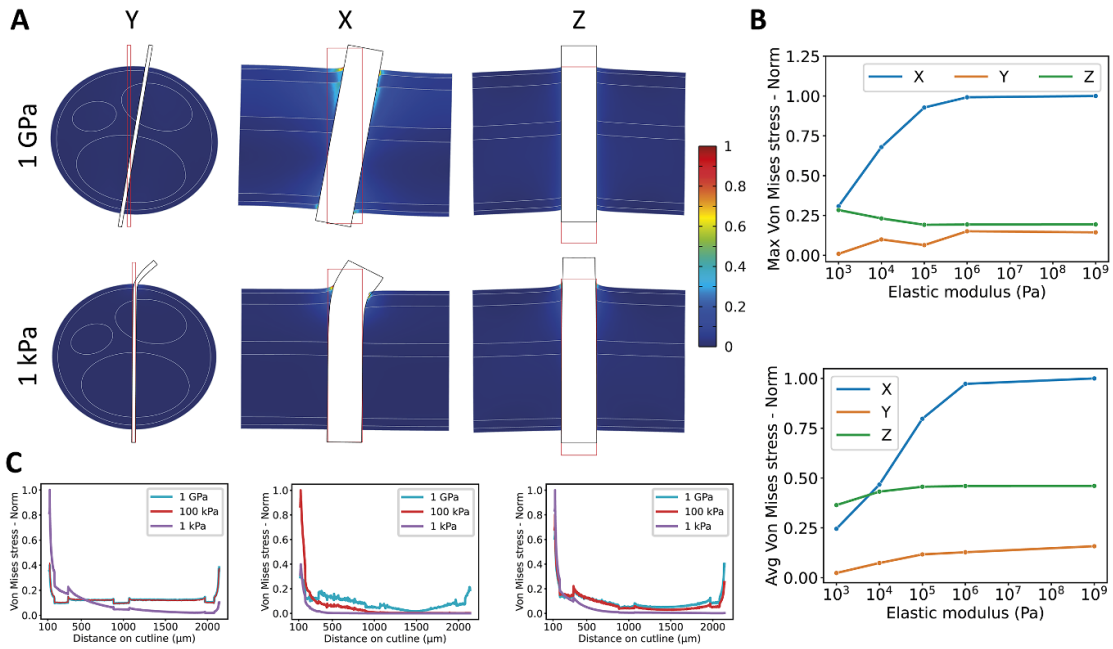


**Figure 2.** (A) Distribution of the normalized Von Mises stress in the deformed nerve following the applied displacement at the top of soft (1 kPa) and stiff (1 GPa) implants along the *X, Y* and *Z* directions. The color bar represents the Von Mises stress, normalized with respect to the maximum value among all of the plots shown (displacement along *X*, modulus of 1 GPa). The maximum values are located at the entry point of the implant and concentrated in few deformed mesh elements. The red contour lines indicate the original position of the implant before the application of any displacement at the top. Deformations are amplified by a factor of 15 for visualization purposes. (B) Plots of the normalized maximum Von Mises stress at the fascicles and average stress at the whole nerve-implant interface with varying bulk elastic moduli. (C) Plot of the distribution of the normalized Von Mises stress along the cutline at the interface in the cross section.

### 3.2. Implant thickness and width

An additional approach to optimize the mechanical properties of penetrating implants consists in changing the aspect ratio of their cross-section, making the device thinner or narrower. This approach has been widely explored with cerebral implants, with the most known example being mesh electrodes [56] and nanowire electrodes [57]. In our simulations we kept the elastic modulus constant to 1 GPa and Poisson ratio of 0.3, associated to the properties of polymers such as polyimide or parylene. We simulated the mechanics of implants with thicknesses of 10, 30 and 50 $\mu$m, respectively. Figures 3(A) and (B) show the distribution of the Von Mises stress across the nerve in the different loading cases and thicknesses together with the trend of the maximum stress in the neighborhood of the implantation site. As expected, the thinnest implant showed the lowest flexural stiffness, therefore bending and concentrating stresses at the entry point when a displacement along the *Y* axis is applied. Moreover, thinner implants cause higher stresses on the nerve when displacements are applied along the *X* or *Z* axes because of their shorter edges. Thinner implants therefore induce stresses up to 60% higher than their thicker equivalents, a result that can be associated to the redistribution of the same forces over smaller and therefore 'sharper' edges. We also evaluated the difference between narrow and large implants, changing their width between 100, 300 and 500 $\mu$m, as shown in figures 3(C) and (D). Our results show that narrower implants cause larger stresses than the larger counterparts, mainly because of the reduced distance between the short sides of the device. Wider devices can reduce peak stresses by up to 40% when considering displacements along *Y*.

### 3.3. Coated implants

Fabricating electrically and mechanically functional implants using only materials with a Young's modulus of 1 kPa is challenging and currently not reported in the literature, we therefore evaluate the effect of the thickness of a soft coating of 1 kPa on the mechanics of a 1 GPa implant. The footprint, that is the total size of the implant, is kept constant while the uniform thickness of the coating is changed between 5 and 22.5 $\mu$m. The plots displayed in figure 4 show the stress distribution across the nerve in each displacement case. The effect of thicker coatings is most visible in the case of the loading in the *Y* direction: this is mostly due to the thinner core lowering the flexural rigidity of the implant in that direction. The bending of the thin-core implant therefore induces higher stresses at the top of the implantation site, while fascicles experience lower values than when using thicker-core devices. In this case the induced stress can be reduced by more than 30% by using a 9:1 coating ratio. When evaluating stimuli in the other directions, the effect of soft coatings becomes more negligible, with reductions in induced stress of up to 15%. To explain such behavior we observe

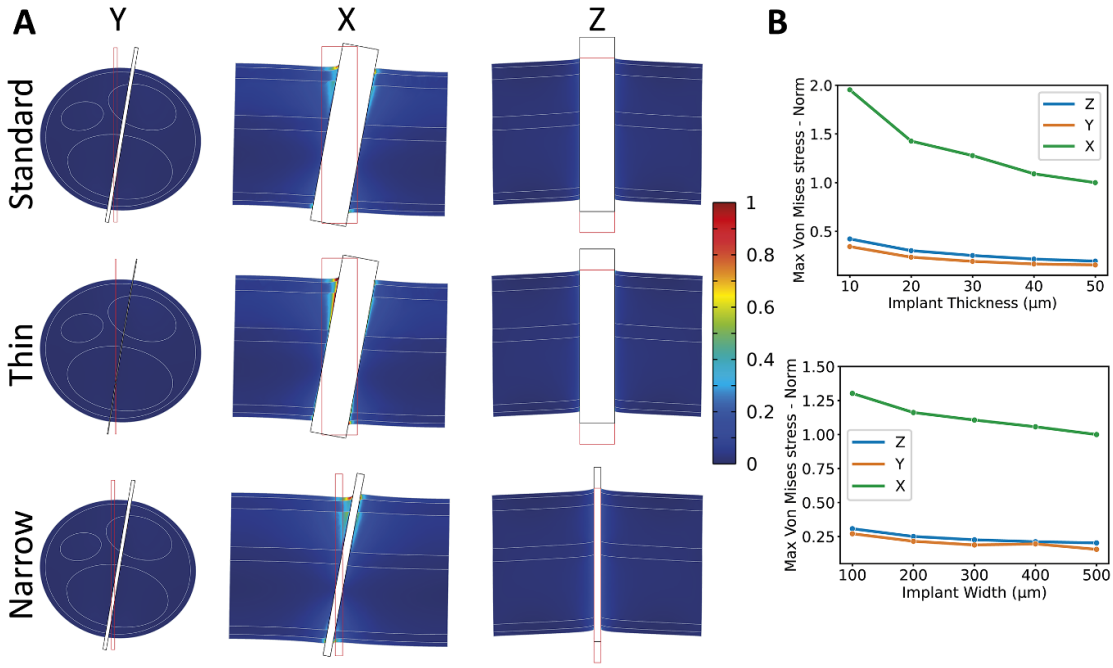


**Figure 3.** (A) Distribution of the normalized Von Mises stress in the deformed nerve following the applied displacement at the top of standard (500 $\mu$m $\times$ 50 $\mu$m), thin (500 $\mu$m $\times$ 10 $\mu$m) and narrow (100 $\mu$m $\times$ 50 $\mu$m) implants along the *X*, *Y* and *Z* directions. The color bar represents the Von Mises stress, normalized with respect to the maximum stress caused by the standard implant (displacement along *X*, modulus 1 GPa). The maximum values are located at the entry point of the implant and concentrated in few deformed mesh elements. The red contour lines indicate the original position of the implant before the application of any displacement at the top. (B) Plot of the normalized maximum Von Mises stress for displacements along the *X*, *Y* and *Z* axis, varying implant thickness (top) and varying implant width (bottom). Deformations are amplified by a factor of 15 for visualization purposes in both (A) and (C).

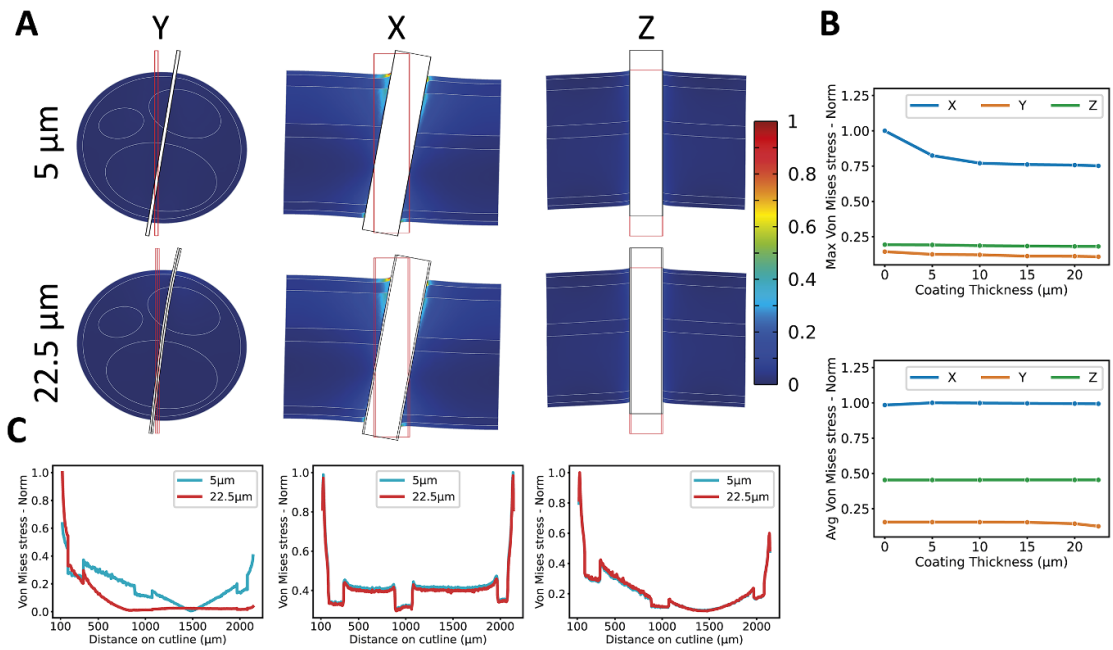


**Figure 4.** (A) Distribution of the normalized Von Mises stress in the deformed nerve following the applied displacement at the top of implants with thin (5 $\mu$m) and thick (22.5 $\mu$m) coatings, along the *X*, *Y* and *Z* directions. The color bar represents the Von Mises stress, normalized with respect to the maximum value among the three plots. The maximum values are located at the entry point of the implant and concentrated in few deformed mesh elements. The red contour lines indicate the original position of the implant before the application of any displacement. Deformations are amplified by a factor of 15 for visualization purposes. (B) Plots of the normalized maximum Von Mises stress at the fascicles and average stress at the whole nerve-implant interface with varying coating thickness. (C) Plot of the distribution of the normalized Von Mises stress along the cutline at the interface in the cross section.

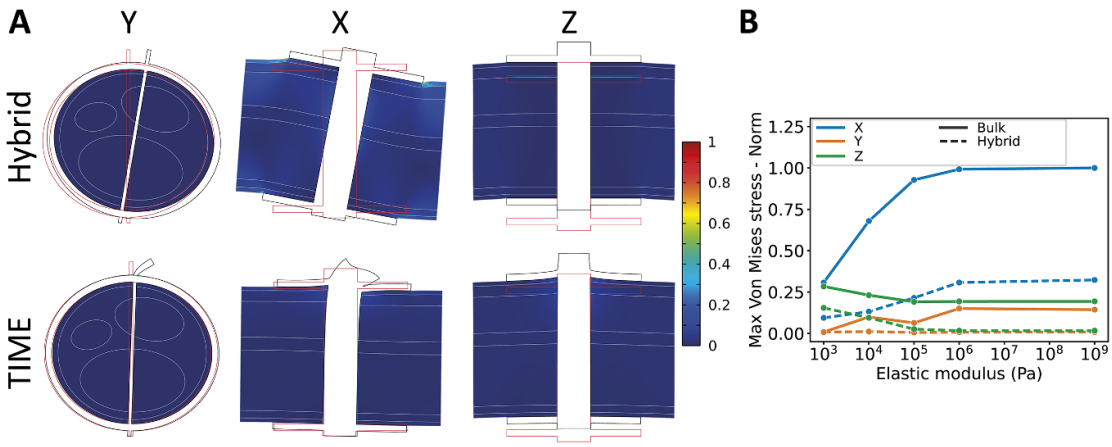


**Figure 5.** (A) Distribution of the normalized Von Mises stress in the deformed nerve following the applied displacement at the top of implants with stiff (1 GPa) TIME and Hybrid implants, along the *X*, *Y* and *Z* directions. The color bar represents the Von Mises stress, normalized with respect to the maximum stress caused by the standard implant (displacement along *X*, modulus 1 GPa). The maximum values are located at the entry point of the implant and concentrated in few deformed mesh elements. The red contour lines indicate the original position of the implant before the application of any displacement. Deformations are amplified by a factor of 15 for visualization purposes. (B) Plot of the normalized maximum Von Mises stress at the fascicles comparing the values when using the TIME and the Hybrid implants at different elastic moduli.

that, in the case of displacements along the length of the nerve, the lower thickness ratio between core and coating in that direction with respect to the same along the *Y* axis makes the bending stiffness almost independent from the thickness of the thin coatings used. Generally, increasing the thickness of the coating reduces the induced stresses and strains on the nerve, although by much less than changing the stiffness of the entire implant.

### 3.4. Hybrid implant

The third model (figure 1) aims at simulating the behavior of a new proposed geometry following the analysis of the results in the TIME implant studies. The goal is to lower the peak stresses applied on the intrafascicular TIME interface by distributing the applied loads on the outer part of the nerve. Figure 5 shows the cross-section of the models representing the normalized stress distribution in the nerves. The deformation displayed in each case shows how the outer structure forces the entire nerve to follow the imparted displacement, therefore lowering the peak applied stresses in the intrafascicular part of the device. The evaluation of the maximum stress values at the penetrating part of the implant and comparing the results with the previously analyzed TIME study reveals the peak stresses caused by the hybrid device are up to 70% lower than the ones caused by the standard penetrating implant, even when using stiffer materials such as standard elastomers (∼1 MPa). The largest improvement is appreciable when *X* displacements are applied, which was the worst case scenario in the previous simulations. In the case of displacements along the *Y*-axis, the reduction can amount to 50%. The plot showing the maximum stress as a function of displacement direction, implant modulus and design, highlights how the advantages brought by the hybrid design are most relevant when using stiffer materials, in the order of MPa, as the rigidity of the structure allows an efficient distribution of the load around the external surface of the nerve. The cutline plots show how softer implants induce higher stresses at the top, due to the implant's deformation. It is also important to notice that stiffer implants may generate stress concentration points at the lateral extremities of the cuff component: to better understand this aspect, we evaluated the maximum stress in the fascicles 400 $\mu$m distally and proximally to the cuff's edges. In the case of displacements along the *X*-axis, the maximum stresses at the edges are 50% lower than the ones at the intrafascicular interface. However, in the other two displacement cases, along *Y* and *Z*, the stresses are double and 50% higher. Nonetheless, the hybrid design can still drastically reduce the applied stresses at the intrafascicular interface, potentially minimizing the scar tissue formation on the long term.

## 4. Discussion

The results obtained in the FEM studies have highlighted interesting features that can guide the design process of less invasive penetrating PNIs.

The FEM studies focusing on the effects of the elastic modulus of the TIMEs have shown that the maximum stress and strain on the nerve can be reduced by using materials with Young's modulus lower than 100 kPa. Moreover, the simulations have shown that softer materials tend to concentrate stresses closer to the stimulus source (the connector), lowering the load on the more sensitive fascicles. Previous experimental studies have highlighted enlarged scarring at the penetration point of the implant, agreeing with our results [15, 43]. The different load

cases analyzed here have also shown that the highest stresses are caused by displacements along the nerve's length, that in turn induced the highest concentration on the short side of the implant. The results indicate an interesting relationship between implant modulus and stresses induced on the nerve. The results show that only a stiffness mismatch of less than three orders of magnitude between nerve and implant can reduce the FBR caused by the stresses induced on the nerve. This indicates that polymeric materials such as polyimides or silicones such as polydimethylsiloxane (PDMS) (Young's modulus > 1 MPa) might not be soft enough to reduce the mechanically-induced scarring. Alternatively, materials such as softer elastomers [58] and hydrogels would be promising candidates in the same challenge. However, the fabrication, implantation, and interfacing of soft PNIs require novel technologies that allow reliable handling, insertion into nerves and connection to external electronics: in this case, there is a growing body of works providing inspiring examples of soft penetrating brain implants based on elastomers and hydrogels [41, 59, 60]. While these studies are based on simplified linear mechanics and assume complete adhesion between nerve and implant, they provide a starting point for the investigation of the most suitable materials or the fabrication of minimally invasive PNIs. In summary, our work provides a comprehensive set of guidelines for the design of minimally invasive neural implants. Our results still agree with the hypothesis on the key role of device stiffness for the reduction of the FBR [61], with the addition of a threshold value that can be used as a guide for future implant design choices.

The models focusing on the aspect ratio of the implant have shown that thinner implants have lower flexural rigidity and can therefore bend under loads along the $Y$ axis, reducing the stresses and strains on the internal fascicles. On the other hand, they cause also higher stresses under loads along the length of the nerve, as they can be considered 'sharper' implants. Similarly, wider implants generally cause lower stresses thanks to the larger interfacial area allowing for the redistribution of stresses. Moreover, the active sites in narrower implants (e.g. twice the width of the openings) would be closer to the sharp edges where scarring would be more pronounced, possibly worsening the electrical performance of the device. Narrower implants are also more likely to twist because of their small aspect ratio, potentially hindering the consistent placement of the device and lowering the reliability of the acquired or applied signals. Changing the aspect ratio of the implants, especially through thinning, seems an interesting route to explore despite the tradeoff between the stresses induced by the device displacements along the $X$ and $Y$ axes. However, the aspect ratio of the implants is limited by the fabrication technology and the required mechanical properties for reliable handling and implantation: for example, overly thin implants might become fragile and prone to breakage but also more sensitive to corrosion and electrical failure. Some mitigation strategies, such as soft coatings, can be envisioned to reduce the stresses caused by axial loads, this without compromising the reduced flexural rigidity. Additionally, while our work focuses on the mechanical interaction between nerve and electrodes of different dimensions at a macroscopic level, it is well known that implant size also influences the response of the immune system at a cellular level, reducing the chronic FBR [56, 62].

Analyzing the properties of uniformly soft-coated implants, we have shown that thicker coatings (at least four times thicker than the core) provide large reductions (up to 30% for displacements along the $Y$ axis) in induced stresses and strains. The benefits associated to uniformly coated implants are most appreciable in the direction of the shortest side. However, compared to thin uniform implants, the presence of the coating reduces the stresses caused by implant motion along the length of the nerve ($X$-axis) by up to 25%. This therefore indicates that coatings can enable the benefits of lower flexural rigidity together with a mitigated implant 'sharpness' on the smallest side of the device. Despite the absence of examples of soft coated intrafascicular implants in current literature, our results suggest that soft coatings on stiffer and thinner intrafascicular implants represent an alternative solution to manufacturing entirely soft devices, that can pose significant challenges in fabrication, handling, and interfacing. Still, in this case, careful engineering of tough soft coatings with reliable adhesion to the implant is required, all while reducing any hindrance on the electrical performance of the device.

The FEM studies on the novel Hybrid TIME geometry have shown that the addition of an extraneural cuff can be an alternative solution to reduce stresses induced by penetrating PNIs. Stresses on the internal part of the nerve can be reduced by up to 60% thanks to the redistribution on the external epineurium made possible by the cuff component. The highest impact on the induced stresses is visible when considering displacements along the length of the nerve, that was the worst-case scenario in the TIME implant simulations. Our simulations support the possibility of an alternative approach to reduce the stresses induced on the nerve, without changing materials. Indeed, the benefits of the hybrid design are also appreciable with elastic moduli higher than 100 kPa, enabling higher flexibility in the choice of materials. The presence of an additional cuff component and its consequent advantages indicate that an intelligent design and anchoring of the implant can drastically reduce the negative effects linked to the mechanical mismatch. However, this innovative design introduces additional challenges such as greater fabrication complexity, longer and more delicate implantation surgeries

and the need of more advanced interfacing electronics. Also, the additional stresses at the extraneural component of the implant could cause the formation of scar tissue around the implant, even if far from the intrafascicular interface. This side effect could be reduced by introducing softer materials at the edges, designing longer extraneural sections or patterning the edges to reduce the resistance to folding. Our work hints at the unexplored potential of mechanical FEM studies to evaluate innovative PNI designs, as we provide the first example of geometrical optimization to reduce induced stresses on the internal part of the nerve. While few examples of fabricated and tested hybrid implants are available in literature [63–65], our work highlights the potential of new designs to reduce the effect of mechanical mismatch and improve long term longevity. Moreover, the presence of an additional extraneural support layer has proven to be beneficial to the chronic mechanical stability of other intrafascicular implants such as the Utah Slanted Electrode Arrays [9, 66]. Although our simulations only focus on the improved mechanical properties of a hybrid design, they do not exclude the additional stimulation and recording capabilities of the same implant: in fact, active sites could be also placed on the extraneural part, providing additional recording and stimulation degrees of freedom in a single device. Overall, our study could also inspire additional design strategies to reduce the stresses induced in the nerve: for example, the wiring should be placed as flush as possible with respect to the surface of the nerve, to minimize the interaction with the surrounding muscles and tissues. Otherwise, as we suppose that the motion is displacement-driven, stress-relieving structures could be integrated in close proximity to the implant through serpentine designs or the integration of soft stretchable materials with the cabling. Finally, when implanting PNIs in large animal models, the cabling could be anchored to bones to compensate for the broad range of motion characteristic of these cases.

It is however important to consider the intrinsic limitations of our study: we decided to consider implant micromotion, originating from the wiring, as the source of the external forces acting on the interface and we therefore approximated the mechanics of the nerve using linearly elastic materials whose properties were derived through micro-scale measurements. This implies that no rate-dependent effects are evaluated and no non-linear mechanics, such as hyperelasticity, are included in the model despite the nerve being a tissue with extremely complex mechanics. We also considerably simplified the geometry of both nerve and implant for the sake of shorter run times, it must be considered that nerves operate in a complex environment, surrounded by moving muscles, connective tissue, and blood vessels. While considering these aspects is essential in designing less invasive PNIs, including all these features into a single model would prove overly tedious for the possible benefits. It is also important to note that our models study the implant-nerve mechanical interaction in one possible geometrical configuration: in reality, fascicular orientation is hard to grasp during implantation in the operating room and multiple scenarios could arise where the device can penetrate any number of fascicles. Therefore, targeted nerve and implant-specific models entailing a larger set of possible implantation configurations would be desirable. Other simplifications, such as the nerve-implant full adhesion, are chosen to set a worst-case scenario with respect to the possible real case: this to obtain more conservative design guidelines that could still prove useful in the reduction of stresses at the interface. This approach however also could make thresholds overly stringent and may unnecessarily complicate the entire implant design, fabrication, and testing pipeline. The absolute values of the applied stresses at the nerve-implant interface depend on the nerve's elastic modulus, that is itself a function of the animal model, age, health condition and more. We have therefore decided to evaluate the relative variation of the stresses, normalizing the results obtained across the different displacement cases, losing therefore the absolute value information. Moreover, there is no consensus yet on whether there exist mechanical stress thresholds that trigger immune reaction mechanisms in the peripheral nerve, making the quantification of these stresses in our model not necessary for the moment. Concerning the nature of the implant's movement, whether translational or rotational, these are not clearly distinguishable in the regime of small displacements we considered. Moreover, this is highly dependent on the implant design and routing of the connecting wires.

## 5. Conclusion

Our work represents the first example of a model on the mechanical interaction between intrafascicular peripheral nerve implants and their hosts. Here we show how the stresses induced at the interface may be reduced by multiple approaches: reducing the mechanical mismatch using softer implants, introducing soft coatings, changing the aspect ratio or the entire geometry of the implant to carefully redistribute the stresses on the nerve. Properly tuning these properties could render implants stealthier and able to seamlessly biointegrate into the host nerves, improving overall chronic performance. We demonstrate how the results of our simulations can provide information that could guide engineers in making the most promising choices when designing minimally invasive intrafascicular peripheral nerve implants. Specifically, our simulations suggest that that the stresses could be reduced by using materials with

elastic moduli less than three orders of magnitude stiffer that the nerve, using soft coatings on ultra-thin flexible implants or by engineering novel implant geometries that can redistribute external loads on the outer surface of the nerve. We simulated the interaction between nerves and implants simplifying the mechanical properties and geometries of the system, therefore the models can be improved by including viscoelastic or hyperelastic materials, anisotropic mechanics and different friction coefficients between devices and nerve tissues, enabling one to simulate slippage between implant and nerve. Moreover, the model can evolve by using geometries derived from histological images and CT scans and include the effect of the nerve's distal ramifications. This could also enable the development of mechanical models focusing on nerves from other animal models and ultimately humans, that include more fascicles and complex geometries. Also, the interaction with the surrounding environment, such as muscles, skin and bones could be considered and included in the simulations, providing even more realistic study scenarios and more accurate results. Once the mechanics of needle penetration are understood and characterized experimentally, implant insertion could be additionally modeled in the future. This could also enable the study of any possible correlation between simulation results and measured scar size and shape, a feature that could improve accuracy in reducing the FBR in future models. The method could be used also to optimize the design of different implant formats, such cuffs [52, 67], penetrating implants such as the longitudinal intrafascicular electrodes and others [10, 68–70]. Our study shows how mechanical FEM could facilitate the design of more effective and usable PNIs (similarly to electrical models [38]) and contributes a new tool for implant design optimization.

## Data availability statement

The data that support the findings of this study are available upon reasonable request from the authors.

## Acknowledgments

This work was supported by INAIL, the Italian National Institute for Insurance against Work-related Injuries, within the PR19-CR-P2 BIOSUP ("BIOnic Solutions for Urinary impaired People") Project'. The authors would like to acknowledge financial support by the Bertarelli Foundation and the SNSF CHRONOS grant. This project has received funding from the European Union's Horizon 2020 research and innovation programme under the Marie Skłodowska-Curie Grant Agreement No. 754354 and by the EU Horizon 2020 research and innovation programme under Grant Agreement No. 813713 (NeuTouch).

## ORCID iDs

Outman Akouissi https://orcid.org/0000-0001-9436-294X
Stéphanie P Lacour https://orcid.org/0000-0001-9075-4022
Silvestro Micera https://orcid.org/0000-0003-4396-8217
Antonio DeSimone https://orcid.org/0000-0002-2632-3057

## References

[1] Charkhkar H, Christie B P, Pinault G J, Tyler D J and Triolo R J 2019 A translational framework for peripheral nerve stimulating electrodes: reviewing the journey from concept to clinic *J. Neurosci. Methods* **328** 108414
[2] Yildiz K A, Shin A Y and Kaufman K R 2020 Interfaces with the peripheral nervous system for the control of a neuroprosthetic limb: a review *J. NeuroEng. Rehabil.* **17** 43
[3] Bensmaia S J, Tyler D J and Micera S 2020 Restoration of sensory information via bionic hands *Nat. Biomed. Eng.* 1–13
[4] Cracchiolo M, Ottaviani M M, Panarese A, Strauss I, Vallone F, Mazzoni A and Micera S 2021 Bioelectronic medicine for the autonomic nervous system: clinical applications and perspectives *J. Neural Eng.* **18** 041002
[5] Paggi V, Akouissi O, Micera S and Lacour S P 2021 Compliant peripheral nerve interfaces *J. Neural Eng.* **18** 031001
[6] Larson C E and Meng E 2020 A review for the peripheral nerve interface designer *J. Neurosci. Methods* **332** 108523
[7] Boretius T, Badia J, Pascual-Font A, Schuettler M, Navarro X, Yoshida K and Stieglitz T 2010 A transverse intrafascicular multichannel electrode (TIME) to interface with the peripheral nerve *Biosens. Bioelectron.* **26** 62–69
[8] Cutrone A, Valle J D, Santos D, Badia J, Filippeschi C, Micera S, Navarro X and Bossi S 2015 A three-dimensional self-opening intraneural peripheral interface (SELINE) *J. Neural Eng.* **12** 016016
[9] Clark G A, Ledbetter N M, Warren D J and Harrison R R 2011 Recording sensory and motor information from peripheral nerves with utah slanted electrode arrays *Annu. Int. Conf. IEEE Eng. Med. Biol. Soc.* vol 2011 pp 4641–4
[10] Yoshida K *et al* 2000 Development of the thin-film longitudinal intra-fascicular electrode *Proc. 5th Annu. Conf. Int. Funct. Electr. Stimul. Soc.* (*January*)
[11] Pohlmeyer E A, Jordon L R, Kim P and Miller L E 2009 A fully implanted drug delivery system for peripheral nerve blocks in behaving animals *J. Neurosci. Methods* **182** 165–71
[12] Michoud F, Sottas L, Browne L E, Asboth L, Latremoliere A, Sakuma M, Courtine G, Woolf C J and Lacour S P 2018 Optical cuff for optogenetic control of the peripheral nervous system *J. Neural Eng.* **15** 015002
[13] Michoud F *et al* 2020 Epineural optogenetic activation of nociceptors initiates and amplifies inflammation *Nat. Biotechnol.* **39** 179–85
[14] Badia J, Boretius T, Pascual-Font A, Udina E, Stieglitz T and Navarro X 2011 Biocompatibility of chronically implanted transverse intrafascicular multichannel electrode (TIME) in the rat sciatic nerve *IEEE Trans. Biomed. Eng.* **58** 2324–32
[15] Christensen M B, Pearce S M, Ledbetter N M, Warren D J, Clark G A and Tresco P A 2014 The foreign body response to the utah slant electrode array in the cat sciatic nerve *Acta Biomater.* **10** 4650–60
[16] Grill W M and Mortimer J T 2000 Neural and connective tissue response to long-term implantation of multiple contact nerve cuff electrodes *J. Biomed. Mater. Res.* **50** 215–26

[17] Renz A F, Reichmuth A M, Stauffer F, Thompson-Steckel G and Vörös J 2018 A guide towards long-term functional electrodes interfacing neuronal tissue *J. Neural Eng.* **15** 061001
[18] ISO 10993-6:2016(en) 2016 *Biological evaluation of medical devices—part 6: tests for local effects after implantation* (available at: www.iso.org/obp/ui#iso:std:iso:10993:-6:ed-3:v1:en) (Accessed 31 May 2021)
[19] Čvančara P *et al* 2020 Stability of flexible thin-film metallization stimulation electrodes: analysis of explants after first-in-human study and improvement of *in vivo* performance *J. Neural Eng.* **17** 046006
[20] Tang L and Eaton J W 1999 Natural responses to unnatural materials: a molecular mechanism for foreign body reactions *Mol. Med.* **5** 351–8
[21] Sheikh Z, Brooks P J, Barzilay O, Fine N and Glogauer M 2015 Macrophages, foreign body giant cells and their response to implantable biomaterials *Materials* **8** 5671–701
[22] Del Valle J, de la Oliva N, Muller M, Stieglitz T and Navarro X 2015 Biocompatibility evaluation of parylene C and polyimide as substrates for peripheral nerve interfaces *2015 7th Int. IEEE/EMBS Conf. on Neural Engineering (NER)* (*Montpellier, France*) (*April*) pp 442–5
[23] Stieglitz T, Schuettler M, Rubehn B, Boretius T, Badia J and Navarro X 2011 Evaluation of polyimide as substrate material for electrodes to interface the peripheral nervous system *2011 5th Int. IEEE/EMBS Conf. on Neural Engineering* (*Cancun*) (*April*) pp 529–33
[24] González-González M A *et al* 2018 Thin film multi-electrode softening cuffs for selective neuromodulation *Sci. Rep.* **8** 1–15
[25] Liu J *et al* 2020 Fully stretchable active-matrix organic light-emitting electrochemical cell array *Nat. Commun.* **11** 3362
[26] Cuttaz E A, Chapman C A R, Syed O, Goding J A and Green R A 2021 Stretchable, fully polymeric electrode arrays for peripheral nerve stimulation *Adv. Sci.* **8** 2004033
[27] Restaino S M, Abliz E, Wachrathit K, Krauthamer V and Shah S B 2014 Biomechanical and functional variation in rat sciatic nerve following cuff electrode implantation *J. NeuroEng. Rehabil.* **11** 73
[28] Lacour S P, Courtine G and Guck J 2016 Materials and technologies for soft implantable neuroprostheses *Nat. Rev. Mater.* **1** 1–14
[29] Liu Y *et al* 2019 Soft and elastic hydrogel-based microelectronics for localized low-voltage neuromodulation *Nat. Biomed. Eng.* **3** 58–68
[30] Zheng X, Woeppel K M, Griffith A Y, Chang E, Looker M J, Fisher L E, Clapsaddle B J and Cui X T 2019 Soft conducting elastomer for peripheral nerve interface *Adv. Healthcare Mater.* **8** 1801311
[31] Carnicer-Lombarte A *et al* 2019 Mechanical matching of implant to host minimises foreign body reaction Bioengineering *bioRxiv preprint* (https://doi.org/10.1101/829648)
[32] Macron J, Gerratt A P and Lacour S P 2019 Thin hydrogel–elastomer multilayer encapsulation for soft electronics *Adv. Mater. Technol.* **4** 1900331
[33] Trel'ová D *et al* 2019 Soft hydrogel zwitterionic coatings minimize fibroblast and macrophage adhesion on polyimide substrates *Langmuir* **35** 1085–99
[34] Golabchi A, Wu B, Cao B, Bettinger C J and Cui X T 2019 Zwitterionic polymer/polydopamine coating reduce acute inflammatory tissue responses to neural implants *Biomaterials* **225** 119519
[35] Raspopovic S, Capogrosso M and Micera S 2011 A computational model for the stimulation of rat sciatic nerve using a transverse intrafascicular multichannel electrode *IEEE Trans. Neural Syst. Rehabil. Eng.* **19** 333–44
[36] Zelechowski M, Valle G and Raspopovic S 2020 A computational model to design neural interfaces for lower-limb sensory neuroprostheses *J. NeuroEng. Rehabil.* **17** 24
[37] Butson C R, Miller I O, Normann R A and Clark G A 2011 Selective neural activation in a histologically derived model of peripheral nerve *J. Neural Eng.* **8** 036009
[38] Romeni S, Valle G, Mazzoni A and Micera S 2020 Tutorial: a computational framework for the design and optimization of peripheral neural interfaces *Nat. Protocols* **15** 10
[39] Schiefer M A, Triolo R J and Tyler D J 2008 A model of selective activation of the femoral nerve with a flat interface nerve electrode for a lower extremity neuroprosthesis *IEEE Trans. Neural Syst. Rehabil. Eng.* **16** 195–204
[40] Subbaroyan J, Martin D C and Kipke D R 2005 A finite-element model of the mechanical effects of implantable microelectrodes in the cerebral cortex *J. Neural Eng.* **2** 103–13
[41] Nguyen J K, Park D J, Skousen J L, Hess-Dunning A E, Tyler D J, Rowan S J, Weder C and Capadona J R 2014 Mechanically-compliant intracortical implants reduce the neuroinflammatory response *J. Neural Eng.* **11** 056014
[42] Schmalbruch H 1986 Fiber composition of the rat sciatic nerve *Anat. Rec.* **215** 71–81
[43] Wurth S *et al* 2017 Long-term usability and bio-integration of polyimide-based intra-neural stimulating electrodes *Biomaterials* **122** 114–29
[44] Kim T-W, Lee J-S, Kim Y-C, Joo Y-C and Kim B-J 2019 Bending strain and bending fatigue lifetime of flexible metal electrodes on polymer substrates *Materials* **12** 15
[45] Chang C-T, Chen Y-H, Lin -C-C K and Ju M-S 2015 Finite element modeling of hyper-viscoelasticity of peripheral nerve ultrastructures *J. Biomech.* **48** 1982–7
[46] Millesi H, Zöch G and Reihsner R 1995 Mechanical properties of peripheral nerves *Clin. Orthop.* **314** 76–83
[47] Tillett R L, Afoke A, Hall S M, Brown R A and Phillips J B 2004 Investigating mechanical behaviour at a core–sheath interface in peripheral nerve *J. Peripher. Nervous Syst.* **9** 255–62
[48] Ma Z, Hu S, Tan J S, Myer C, Njus N M and Xia Z 2013 *In vitro* and *in vivo* mechanical properties of human ulnar and median nerves *J. Biomed. Mater. Res.* A **101A** 2718–25
[49] Chen R-J, Lin -C-C K and Ju M-S 2010 *In situ* biomechanical properties of normal and diabetic nerves: an efficient quasi-linear viscoelastic approach *J. Biomech.* **43** 1118–24
[50] Alvey L M, Jones J F X, Tobin-O'Brien C and Pickering M 2019 Bands of fontana are caused exclusively by the sinusoidal path of axons in peripheral nerves and predict axon path; evidence from rodent nerves and physical models *J. Anat.* **234** 165–78
[51] Giannessi E, Stornelli M R, Coli A and Sergi P N 2019 A quantitative investigation on the peripheral nerve response within the small strain range *Appl. Sci.* **9** 6
[52] Delianides C, Tyler D, Pinault G, Ansari R and Triolo R 2020 Implanted high density cuff electrodes functionally activate human tibial and peroneal motor units without chronic detriment to peripheral nerve health *Neuromodulation* **23** 754–62
[53] McKee C T, Last J A, Russell P and Murphy C J 2011 Indentation versus tensile measurements of Young's modulus for soft biological tissues *Tissue Eng.* B **17** 155–64
[54] Rosso G and Guck J 2019 Mechanical changes of peripheral nerve tissue microenvironment and their structural basis during development *APL Bioeng.* **3** 036107
[55] Carnicer Lombarte A 2019 Mechanically compliant coatings in neural implants as a strategy to reduce foreign body reaction in the peripheral nervous system *PhD Thesis* University of Cambridge, Clinical Neurosciences (https://doi.org/10.17863/CAM.37929)
[56] Zhou T, Hong G, Fu T-M, Yang X, Schuhmann T G, Viveros R D and Lieber C M 2017 Syringe-injectable mesh electronics integrate seamlessly with minimal chronic immune response in the brain *Proc. Natl Acad. Sci.* **114** 5894–9

[57] Vitale F et al 2018 Fluidic microactuation of flexible electrodes for neural recording *Nano Lett.* **18** 326–35
[58] Heinrichs V, Dieluweit S, Stellbrink J, Pyckhout-Hintzen W, Hersch N, Richter D and Merkel R 2018 Chemically defined, ultrasoft PDMS elastomers with selectable elasticity for mechanobiology *PLoS One* **13** e0195180
[59] Du Z J, Kolarcik C L, Kozai T D Y, Luebben S D, Sapp S A, Zheng X S, Nabity J A and Cui X T 2017 Ultrasoft microwire neural electrodes improve chronic tissue integration *Acta Biomater.* **53** 46–58
[60] Zhang E N, Clément J-P, Alameri A, Ng A, Kennedy T E and Juncker D 2021 Mechanically matched silicone brain implants reduce brain foreign body response *Adv. Mater. Technol.* **6** 2000909
[61] Carnicer-Lombarte A, Chen S-T, Malliaras G G and Barone D G 2021 Foreign body reaction to implanted biomaterials and its impact in nerve neuroprosthetics *Front. Bioeng. Biotechnol.* **9** 1–22
[62] Luan L et al 2017 Ultraflexible nanoelectronic probes form reliable, glial scar–free neural integration *Sci. Adv.* **3** e1601966
[63] Tyler D J and Durand D M 1997 A slowly penetrating interfascicular nerve electrode for selective activation of peripheral nerves *IEEE Trans. Rehabil. Eng.* **5** 51–61
[64] Ranieri A, Andersen R E, Lauridsen M V and Harreby K R 2014 A combined interfascicular-cuff electrode (ICE) for selective recruitment of polyfascicular peripheral nerves using transversal stimulation *Replace, Repair, Restore, Relieve—Bridging Clinical and Engineering Solutions in Neurorehabilitation* vol 7, ed W Jensen, O K Andersen and M Akay (Cham: Springer International Publishing) pp 685–94
[65] Kim H et al 2020 Cuff and sieve electrode (CASE): the combination of neural electrodes for bi-directional peripheral nerve interfacing *J. Neurosci. Methods* **336** 108602
[66] Wendelken S, Page D M, Davis T, Wark H A C, Kluger D T, Duncan C, Warren D J, Hutchinson D T and Clark G A 2017 Restoration of motor control and proprioceptive and cutaneous sensation in humans with prior upper-limb amputation via multiple utah slanted electrode arrays (USEAs) implanted in residual peripheral arm nerves *J. NeuroEng. Rehabil.* **14** 1–17
[67] Forssell M et al 2019 Compliant adhesive cuff electrode for selective stimulation in rat vagus nerve *2019 IEEE SENSORS* (*Montreal, QC, Canada*) (*October*) pp 1–4
[68] Koppaka S, Hess-Dunning A and Tyler D J 2021 Directed stimulation with interfascicular interfaces for peripheral nerve stimulation *J. Neural Eng.* **18** 066006
[69] Kim O et al 2017 Novel neural interface electrode array for the peripheral nerve *2017 Int. Conf. on Rehabilitation Robotics (ICORR)* (*July*) pp 1067–72
[70] Strauss I et al 2020 Q-PINE: a quick to implant peripheral intraneural electrode *J. Neural Eng.* **17** 066008